

## Article

# Influence of Cross-Sectional Shape on Flow Capacity of Open Channels

Chunlin Qiu <sup>1</sup>, Shihe Liu <sup>1,\*</sup>, Jiesheng Huang <sup>1</sup>, Wenhao Pan <sup>2</sup> and Rui Xu <sup>3</sup>

<sup>1</sup> State Key Laboratory of Water Resources and Hydropower Engineering Science, Wuhan University, Wuhan 430072, China; qiuchunlin@whu.edu.cn (C.Q.); sdjshuang@whu.edu.cn (J.H.)

<sup>2</sup> Changjiang Institute of Survey, Planning, Design and Research, Wuhan 430010, China; panwenhao@whu.edu.cn

<sup>3</sup> Tianjin Research Institute for Water Transport Engineering, M.O.T., Tianjin 300456, China; x987654r@163.com

\* Correspondence: shiheliu@126.com

**Abstract:** Open-channel flow can be easily found in nature and engineering projects, and the channels' cross-sections are of various shapes. Research on the flow capacity of open channels with different cross-sections can help deepen our understanding of the dependence of open channels' general characteristics on cross-sectional shapes at a theoretical level. Furthermore, it has potential practical value in engineering projects. Through theoretical analysis, experimental research, and numerical calculation, two conclusions can be drawn in the present article: (1) A general expression for flow capacity was deduced based on viscous fluid theory, and a parameter describing the influence of cross-sectional shapes on flow capacity,  $C_Q$ , was obtained. The advantage of our method is that the expression can be used to calculate the parameter directly, which varies with general and flow field characteristics. Another advantage is that the parameter can describe general and flow field characteristics in a uniform way. (2) The width-to-wetted perimeter ratio was selected to describe the cross-sectional shapes. The dependence of the parameter,  $C_Q$ , on cross-sectional shapes can be summarized as follows: In laminar flow, the parameter depends on the width-to-wetted perimeter ratio only. In turbulent flow at a medium or low Reynolds number, the parameter varied with width-to-wetted perimeter ratio and Reynolds number. In turbulent flow at a high Reynolds number, the parameter was independent of the width-to-wetted perimeter ratio.

**Keywords:** open-channel flow; cross-sectional shape; flow capacity; width-to-wetted perimeter ratio; Reynolds number



**Citation:** Qiu, C.; Liu, S.; Huang, J.; Pan, W.; Xu, R. Influence of Cross-Sectional Shape on Flow Capacity of Open Channels. *Water* **2023**, *15*, 1877. <https://doi.org/10.3390/w15101877>

Academic Editors: Cristina Maria Sena Fael, Cátia Sofia Batista Taborda and Hamidreza Rahimi

Received: 14 April 2023

Revised: 5 May 2023

Accepted: 12 May 2023

Published: 16 May 2023



**Copyright:** © 2023 by the authors. Licensee MDPI, Basel, Switzerland. This article is an open access article distributed under the terms and conditions of the Creative Commons Attribution (CC BY) license (<https://creativecommons.org/licenses/by/4.0/>).

## 1. Introduction

Open-channel flow is widely found in nature and engineering projects. Rivers in nature and water conveyance channels in engineering are typical open channels. In hydraulics, the discharge capacity of constant uniform flow in open channels can be calculated as follows. The variables are shown in Figure 1.

$$Q = AC\sqrt{RS_f} \quad (1)$$

where  $Q$  is the discharge capacity ( $\text{m}^3/\text{s}$ );  $A$  is the area ( $\text{m}^2$ );  $R$  is the hydraulic radius ( $\text{m}$ );  $S_f$  is the energy slope (dimensionless); and  $C$  is the Chezy coefficient (dimensionless).

This empirical formula was obtained by Chezy in 1775 based on a large amount of measured data of uniform flow in open channels. The boundary of the artificial channel and the natural channel is varied and there are various cross-sectional shapes in the channels (see Figure 2). On the basis of the theory of open-channel flow, people generally obtain the expression for the flow capacity of the channel with a certain cross-sectional shape through experiments and numerical simulations. However, in nature and engineering, the cross-sectional shape of an open channel varies. Studying only one type of cross-sectional shape

in this manner is feasible; however, extending this to all types of cross-sectional shapes, and for cross-sections with similar shapes, makes the research process challenging and rather cumbersome. At the same time, it is not conducive to the simplicity of engineering calculations. Therefore, it is necessary to find a parameter that can uniformly describe the effect of cross-sectional shape on flow capacity.

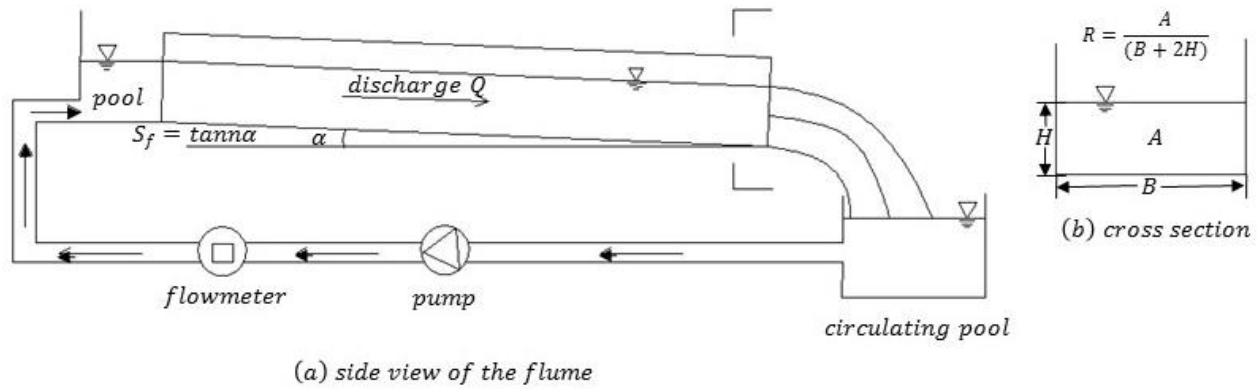


Figure 1. Schematic figure of a flume.

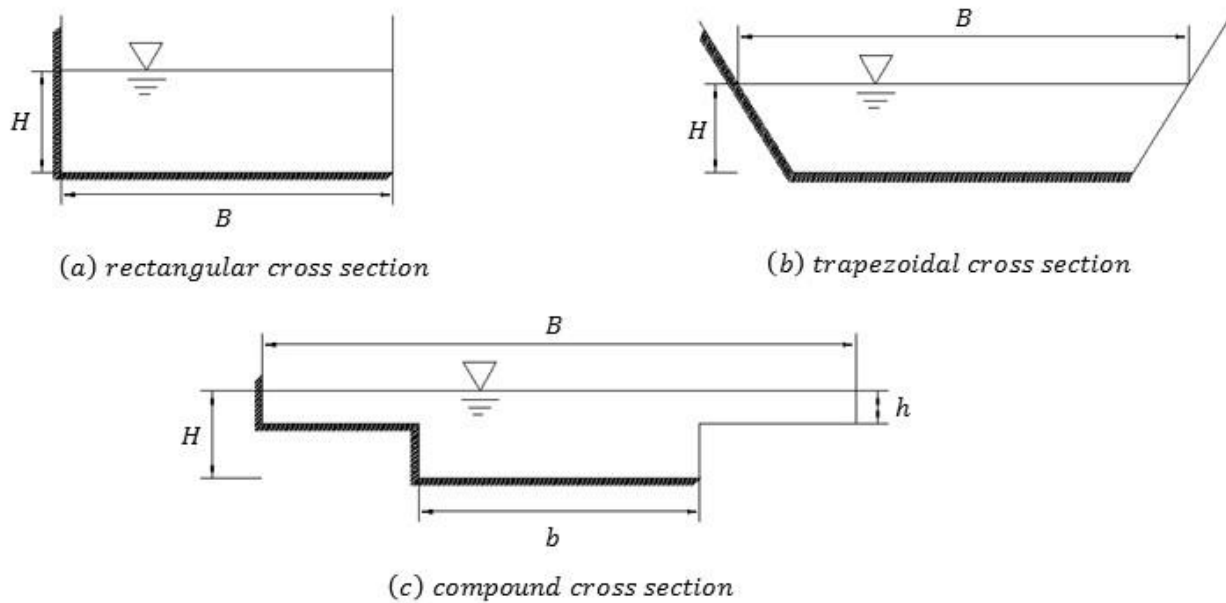


Figure 2. Different cross-sectional shapes in open channels.

As H. Graf [1] pointed out, at present, no parameter can describe the variability of cross-sectional shapes well. In hydraulics, a semi-empirical model is also used to describe this effect; that is, the effects of all shape factors are expressed as parameters. The hydraulic radius commonly used in hydraulics is not sufficient to reflect the influence of cross-sectional shape on flow capacity. Flow capacity is related to energy loss coefficient  $\lambda$ . Therefore, the influence of cross-sectional shape on the energy loss coefficient  $\lambda$  must be considered by multiplying a coefficient  $\varphi$  in front of hydraulic radius  $R$ . The equation is

$$\frac{1}{\sqrt{\lambda}} = -2\log\left(\frac{1}{a_f} \frac{k_s}{\varphi R} + \frac{b_f}{\varphi Re_d \sqrt{\lambda}}\right) \tag{2}$$

where  $\lambda$  is the coefficient of energy loss (dimensionless);  $k_s$  is the rough height (m);  $a_f$  and  $b_f$  are empirical coefficients [2] related to the discharge and operating conditions (dimensionless);  $\varphi$  is a coefficient related to the shape, e.g., for a rectangular section,  $\varphi = 0.95$ ,

for a trapezoidal section,  $\varphi = 0.80$ , and for an equilateral triangle section,  $\varphi = 1.25$ ;  $R$  is the hydraulic radius (m); and  $Re_d = \frac{4RU}{\nu}$ ,  $Re_d$  is the Reynolds number with the hydraulic diameter as the characteristic length.

Parameters are used to reflect the effect of cross-sectional shape. However, different researchers have different opinions on which factors these parameters are related to. The following is a review of the literature on this issue. Cantero et al. [3] showed that the single channel method can be used to estimate discharge capacity. In this method, the equivalent Manning coefficient for the entire cross-section,  $n_e$ , is related to the wetted perimeter (Chow [4]; Prinos and Townsend [5]). Dracos and Hardegger [6] and French [7] used a weighted hydraulic radius to estimate flow discharge using the single channel method. For calculating the discharge of symmetrical flood plains, Cantero et al. [3] provided an expression (Equation (6)) using a flow area  $A$  with a certain weight. This expression is also related to mean flow velocity  $U$ , which is influenced by shape factors such as hydraulic radius, flood plain depth, and wetted perimeter (Wormleaton et al. [8]). Khatua et al. [9] provided expressions of two kinds of wetted perimeter coefficients. The expressions contain the power function of the flow area ratio. The expressions used to calculate the flow rate are complicated (see Cantero et al. [3], Equation (9)). The expressions of the kinetic energy correction coefficient (or Coriolis coefficient)  $\alpha$  and momentum correction coefficient (or Boussinesq coefficient)  $\beta$  are given by Blalock and Sturm [10], Field et al. [11], and Chaudhry and Bhallamudi [12], respectively. Then, the specific energy function  $E$ , momentum function  $S$ , and flow profile  $h = h(x)$  are calculated. The Froude number of compound open channels was approximated by Blalock and Sturm [10], and is related to shape parameters such as top width, wetted perimeter, hydraulic radius of the subsection, etc. This is a bulk cross-sectional Froude number, rather than a local Froude number valid for different points in a section. The bulk cross-sectional Froude number can be used to further calculate the water depth and specific energy (Blalock and Sturm [10]; Blalock and Sturm [13]; and Costabile and Macchione [14]).

In addition, it is not clear how the parameter changes in laminar flow or medium and low Reynolds number flow, or high Reynolds number flow. The following is a review of the literature on this issue. There is little data on the connection between Reynolds number and the parameter that can describe the effect of cross-sectional shapes on discharge capacity. Studies mainly focus on the influence of Reynolds number on characteristic variables, such as velocity and depth, etc. Through smooth flume experiments, Johnson and Cowen [15] found that when the Reynolds number changes from 4950 to 73,800, the velocity index  $k$  changes from 0.82 to 0.93 ( $k = U_b/U_{surf}$ , where  $U_b$  is the depth-averaged velocity and  $U_{surf}$  is the local surface velocity), thus affecting the change in average velocity and discharge capacity. Harpold et al. [16] also observed through experiments that the variation in Reynolds number would affect the variation in the velocity index. The velocity index was set at 0.85 under base flow conditions and 0.93 under high flow conditions. Chen [17] and Schlichting [18] found that the logarithmic law of flow velocity is suitable for high Reynolds number flows, while the power law is valid for lower Reynolds number intervals. The coefficients of these functions are generally obtained experimentally.

Experimental studies and numerical calculations are important means to investigate the parameter that can describe the effect of cross-sectional shapes on discharge capacity. The following is an introduction of related experimental studies and numerical calculations. Some are directly related to parameters, while others are about characteristic variables, such as the energy loss coefficient,  $\lambda$ , and velocity distribution. For example, Tracy et al. [19] carried out a series of experiments to study the influence of the side wall of an open channel on velocity distribution and energy loss. Under the same Reynolds number conditions, the energy loss coefficient of rectangular open-channel flow is slightly higher than that of circular channel flow and rectangular open-channel flow with an infinite width-to-depth ratio. Kirkgöz [20] used a laser Doppler anemometer to measure rectangular open-channel flow with smooth and rough surfaces and analyzed the velocity distribution of cross-sections under different wall conditions. The trapezoidal open-channel flow, compound

open-channel flow, and rectangular open-channel flow with different width-depth ratios were studied in a large number of experiments by researchers. Although the results of experimental research and numerical calculations are abundant, no uniform parameter exists to describe the influence of cross-sectional shapes on the discharge capacity of open channels with regular channel boundary conditions.

Recently, we studied the general description of open-channel flow theoretically, in order to acquire the parameter that can describe the effect of cross-sectional shapes on discharge capacity. Based on the theory of movement of viscous liquids, the governing equations of laminar and turbulent motions of homogeneous incompressible viscous liquid in an open channel were directly integrated to construct new integral and differential models, respectively [21–24]. As a result, a solid theoretical foundation for a general description of open-channel flow in regular boundary conditions was laid. Then, from the perspective of fluid mechanics, we derived the parameter  $C_Q$ , which describes the influence of cross-sectional shape on flow capacity, through backward derivation, generalization, and simplification. The total flow energy equation (one of the governing equations of the integral model) established from the perspective of hydrodynamics solves the following shortcomings in the total flow energy equation in hydraulics: (1) The direct relationship between flow field description in fluid mechanics and total flow description in hydraulics cannot be built. (2) Distinguishing between total flow energy equations in laminar flow conditions and turbulent flow conditions in an open channel is impossible. (3) The effect of viscous dissipation and turbulence on total flow energy loss cannot be calculated directly, so the direct expression of total flow energy loss cannot be given. (4) The pressure on the cross-section must obey the static pressure distribution, but it is difficult to satisfy in the conditions of secondary flow and turbulent flow. This article is based on a new parameter,  $C_Q$ , that can describe the effect of cross-sectional shapes on discharge capacity, and the following work was carried out: (1) The general expression of open-channel flow capacity was deduced firstly through theoretical analysis. At the same time, the expression of the flow capacity coefficient  $C_Q$  was given. (2) On the basis of the general expression, the direct formula for calculating the coefficient of flow capacity,  $C_Q$ , under laminar flow conditions was given. (3) Additionally, on the basis of the general expression, combined with the experimental results of this article and the literature, the variation trend of  $C_Q$  under different turbulent flow conditions was obtained. (4) By means of numerical analysis, the variation trends of  $C_Q$  in rectangular, trapezoidal, and compound open channels were obtained. (5) In the Discussion section, the variation trends of  $C_Q$  in laminar and turbulent zones are shown in the same graph, using the experimental and numerical results. The differences in  $C_Q$  in two regions are discussed. (6) The Conclusion section summarizes the variation trend of  $C_Q$  in laminar, low and medium Reynolds number turbulent region, and high Reynolds number turbulent region. The research objective of this article was achieved; that is, we identified a flow capacity parameter  $C_Q$  to represent the flow discharge capacity. The calculation formula is a direct expression, which is convenient for application in engineering calculations. At the same time, the width-to-wetted perimeter ratio was used to generalize the cross-sectional shape. The variation trend of  $C_Q$  with width-to-wetted perimeter ratio and Reynolds number was obtained.

The results of this study can be used to predict the flow capacity of open channels with different cross-sectional shapes, i.e., to estimate the flow discharges of open channels at different water levels. Hydraulics generally describe the flow capacity using the roughness coefficient  $n$  and the Chezy coefficient  $C$ . However, these are empirical descriptions, not precise expressions of flow capacity. In order to connect the boundary of open channels and flow field, this research was conducted based on coupling the flow field description with the general description. The results of this article can be applied to estimate the discharges at different water levels in open-channel flow with a regular boundary. Natural rivers generally have irregular boundaries. Before using the results of this paper, a generalization of boundary should be conducted first. That is, irregular boundaries are generalized to regular boundaries. Then, the generalized regular boundary can be used to estimate discharge.

## 2. Materials and Methods

### 2.1. Theoretical Analysis

We previously discussed the general description of open-channel flows in laminar and turbulent conditions in the framework of viscous fluid motion [21–24]. The connection between this article and our previous works is that our previous research was about general description and field description. It focused on the coefficient of energy loss,  $\lambda$ . On the basis of our previous results, this article further considers the influence of cross-sectional shapes. The calculation formula of energy (mechanical energy) loss  $h_w$  in the region with volume  $V$  between two cross-sections is (derived from equations in [21–24]):

$$h_w = \begin{cases} \frac{2\nu}{gQ} \iiint_V s_{ij}s_{ij}dV & \text{laminar} \\ \frac{1}{gQ} \iiint_V (2\nu\bar{s}_{ij} - \overline{u'_i u'_j}) \bar{s}_{ij}dV & \text{turbulent} \end{cases} \quad (3)$$

Note: Equations (3), (4), and (8) are all for open flows.

In Equation (3),  $\nu$  is the kinematic viscosity coefficient of liquid ( $\text{m}^2/\text{s}$ );  $g$  is the acceleration of gravity ( $\text{m}/\text{s}^2$ );  $Q$  is the discharge ( $\text{m}^3/\text{s}$ ); and  $s_{ij}$ ,  $\bar{s}_{ij}$ , and  $-\overline{u'_i u'_j}$  represent the velocity variation rate of laminar flow, the time-mean velocity variation rate of turbulent flow, and the Reynolds stress of open channels, respectively. In the condition of constant uniform flow in open channels, the corresponding energy loss coefficient  $\lambda$  can be calculated as follows [24]:

$$\lambda = \begin{cases} \frac{16\nu R}{AU^3} \iint_A s_{ij}s_{ij}dA & \text{laminar} \\ \frac{8R}{AU^3} \iint_A (2\nu\bar{s}_{ij} - \overline{u'_i u'_j}) \bar{s}_{ij}dA & \text{turbulent} \end{cases} \quad (4)$$

In Equation (4),  $\lambda$  is the coefficient of energy loss (dimensionless);  $R$  is the hydraulic radius (m);  $A$  is the discharge section area ( $\text{m}^2$ ); and  $U$  is the mean velocity ( $\text{m}/\text{s}$ ).

For constant uniform flow in open channels, the total flow momentum equation and energy equation are jointly solved to obtain the wetted perimeter-mean shear stress:

$$\tau_0 = \frac{\lambda}{8} \rho U^2 = \rho g \frac{A}{\chi} \frac{h_w}{L} \quad (5)$$

In Equation (5),  $\tau_0$  is the viscous stress on the overflow surface (Pa);  $\rho$  is the fluid density ( $\text{kg}/\text{m}^3$ );  $\chi$  is the wetted perimeter (m); and  $L$  is the distance (m).

Then, the following can be derived:

$$Q = \sqrt{\frac{8g}{\lambda}} A \sqrt{gRS_f} \quad (6)$$

In Equation (6),  $S_f$  is the energy slope (dimensionless).

For uniformly describing the discharge capacity of laminar open flow and turbulent open flow in the hydraulically smooth region, Equation (6) can be rewritten as

$$Q = C_Q Re_R^{1/2} A \sqrt{gRS_f} \quad (7)$$

where  $C_Q$  is the parameter reflecting the influence of the cross-sectional shape on discharge capacity except hydraulic radius (hydraulic radius was used as a parameter on the right side of Equation (7)).  $C_Q$  is expressed as:

$$C_Q = \sqrt{\frac{8}{\lambda Re_R}} = \begin{cases} \sqrt{\frac{AU^2}{2R^2} \frac{1}{\iint_A s_{ij}s_{ij}dA}} & \text{laminar} \\ \sqrt{\frac{AU^3}{R} \frac{Re_R^{-1}}{\iint_A (2\nu\bar{s}_{ij} - \overline{u'_i u'_j}) \bar{s}_{ij}dA}} & \text{turbulent} \end{cases} \quad (8)$$

where  $U$  is the average velocity of the section.  $Re_R = \frac{UR}{\nu}$  where  $Re_R$  is the Reynolds number, with hydraulic radius as the characteristic length scale. Equation (8) has the following advantages: (1) it is a direct expression and can directly describe how the discharge capacity parameter  $C_Q$  varies with the general characteristics (i.e., energy loss coefficient) or flow field characteristics (i.e., time-mean velocity and Reynolds stress). (2) The discharge capacity parameters obtained from the general characteristics and flow field characteristics are consistent. The discharge capacity parameters of laminar flow and turbulent flow in open channels are discussed below.

## 2.2. Laminar Flow in an Open Channel

For laminar flow in a rectangular open channel, the expression of energy loss coefficient is obtained as

$$\lambda = \frac{24}{Re_R} \frac{B^2}{(B + 2H)^2} \frac{1}{1 - \frac{384}{\pi^5} \frac{H}{B} \sum_{m=0}^{\infty} \frac{1}{(2m+1)^5} \tanh \left[ \frac{\pi}{2} \left( m + \frac{1}{2} \right) \frac{B}{H} \right]} \quad (9)$$

where  $B$  and  $H$  represent the width of open channel and flow depth, respectively. Substituting Equation (9) into Equation (8), along with the wetted perimeter  $\chi = B + 2H$ ,  $\frac{B}{H} = \frac{2(B/\chi)}{1 - (B/\chi)}$ , the following equation can be derived:

$$C_Q = \frac{1}{\sqrt{3}} \frac{\chi}{B} \sqrt{1 - \frac{192}{\pi^5} \left( \frac{\chi}{B} - 1 \right) \sum_{m=0}^{\infty} \frac{1}{(2m+1)^5} \tanh \left[ \frac{\pi}{2} (2m+1) \frac{1}{\chi/B - 1} \right]} \quad (10)$$

## 2.3. Experiments for Turbulence in an Open Channel

In order to study the influence of  $C_Q$  on turbulence in an open channel, we performed experiments using a high-precision, varying slope, rectangular smooth flume. The experiment was done in Changjiang River Scientific Research Institute, Wuhan City, China. The experimental device is shown in Figure 3. The flume is 28 m long, 56 cm wide, and 70 cm high. The actual picture and details of the flume are shown in Figure 4. The range of slope variation is  $-1-7\%$ . In this experiment, the bottom slope is 2.5‰ and 5‰. The slope changing system is shown in Figure 4. The frequency converter and needle water level gauge are shown in Figure 5. The flow velocity was measured by acoustic Doppler velocimetry (ADV). The actual picture of the ADV meter is shown in Figure 6. An ultrasonic automatic water level meter was used to measure the water depth. The instrument can synchronously measure the water level at many points, and it can output the results according to the specified format. Figure 7 shows a physical picture of the instrument. In the experiment, seven high-precision ultrasonic water level probes were arranged along the flume (measuring Section 1#–7#, as shown in Figure 3). The installation height was no less than 5 cm from the water surface. The sampling frequency was 10 Hz. The experimental conditions are shown in Table 1. In the experiment, we mainly measured velocity and water depth. The sample size of the data collected via ADV was 1800 PCS/min. Each measuring point was sampled for 1 min, and the sampling signal frequency was 30 signals per second. Table 1 is the experiment conditions.

**Table 1.** Experiment conditions.

Case	Discharge $Q$ (L/s)	Slop $S_f$	Water Depth $H$ (cm)
1	20	0.0025	5.99
2	40	0.0025	9.41
3	60	0.0025	12.30
4	20	0.005	4.48
5	40	0.005	6.86
6	60	0.005	9.06

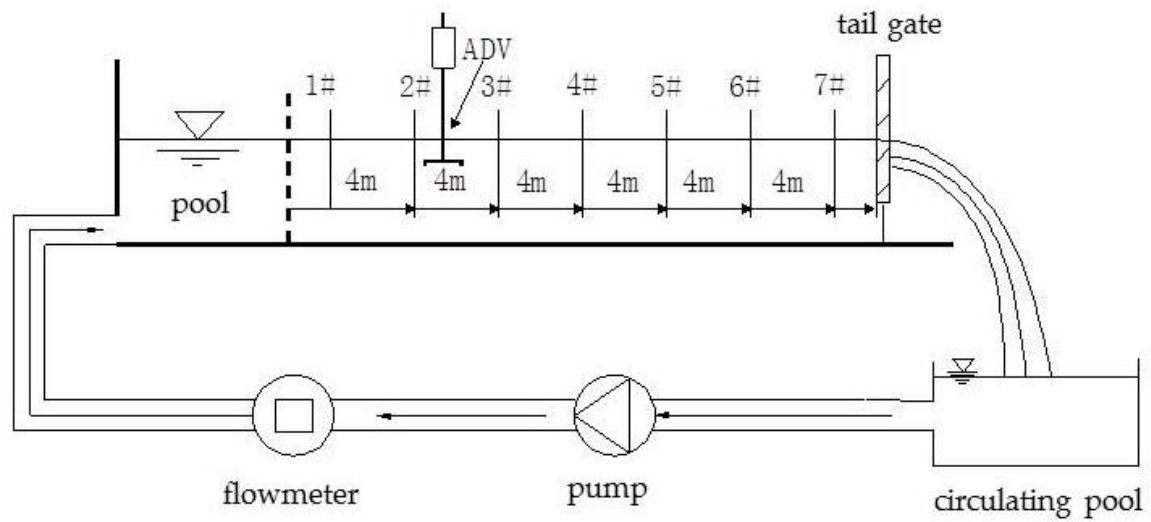
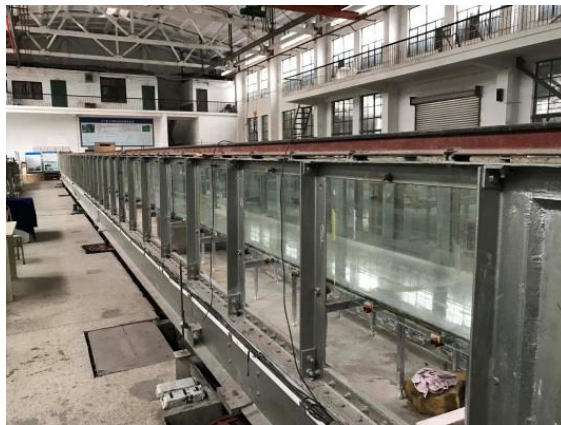
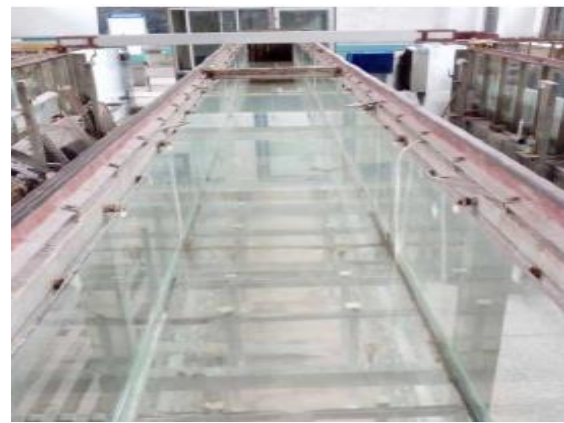


Figure 3. Schematic figure of experimental device.



(a)



(b)



(c)



(d)

Figure 4. Flume in the experiment. (a) Flume side view; (b) top view of flume; (c) inflow system; and (d) slope changing system.

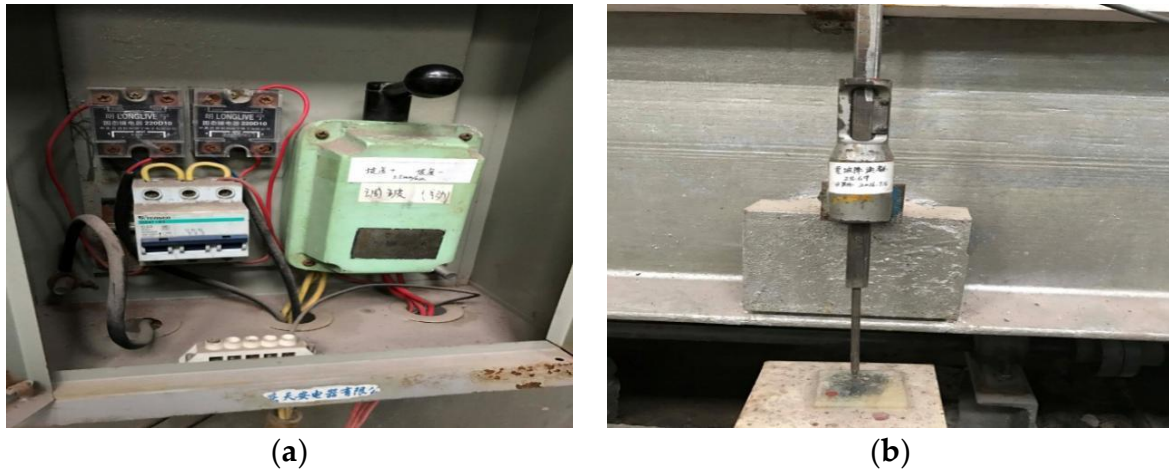


**Figure 5.** Flume in the experiment. (a) Frequency converter (used for controlling the power of the inflow pump); (b) needle water level gauge.



**Figure 6.** Acoustic Doppler Velocimetry (ADV).



**Figure 7.** Ultrasonic automatic water level meter.

### 3. Results

#### 3.1. Laminar Flow in an Open Channel

Figure 8 shows the variation in discharge capacity parameter  $C_Q$  with width-to-wetted perimeter ratio  $B/\chi$ . The numerical value is the result calculated using Equation (8) (or Equation (10)). The “laminar” expression in Equation (8) (or Equation (10)) and Figure 6 show that  $C_Q$  is independent of the Reynolds number in laminar flow but strongly dependent only on  $B/\chi$ . With the increase in  $B/\chi$ ,  $C_Q$  gradually decreased. The numerical results in Figure 8 were fitted to derive an approximate calculation formula shown in Equation (11). The fitting results are shown in Figure 8.

$$C_Q = -0.5174(B/\chi)^2 + 0.3869(B/\chi) + 0.6877 \quad (11)$$

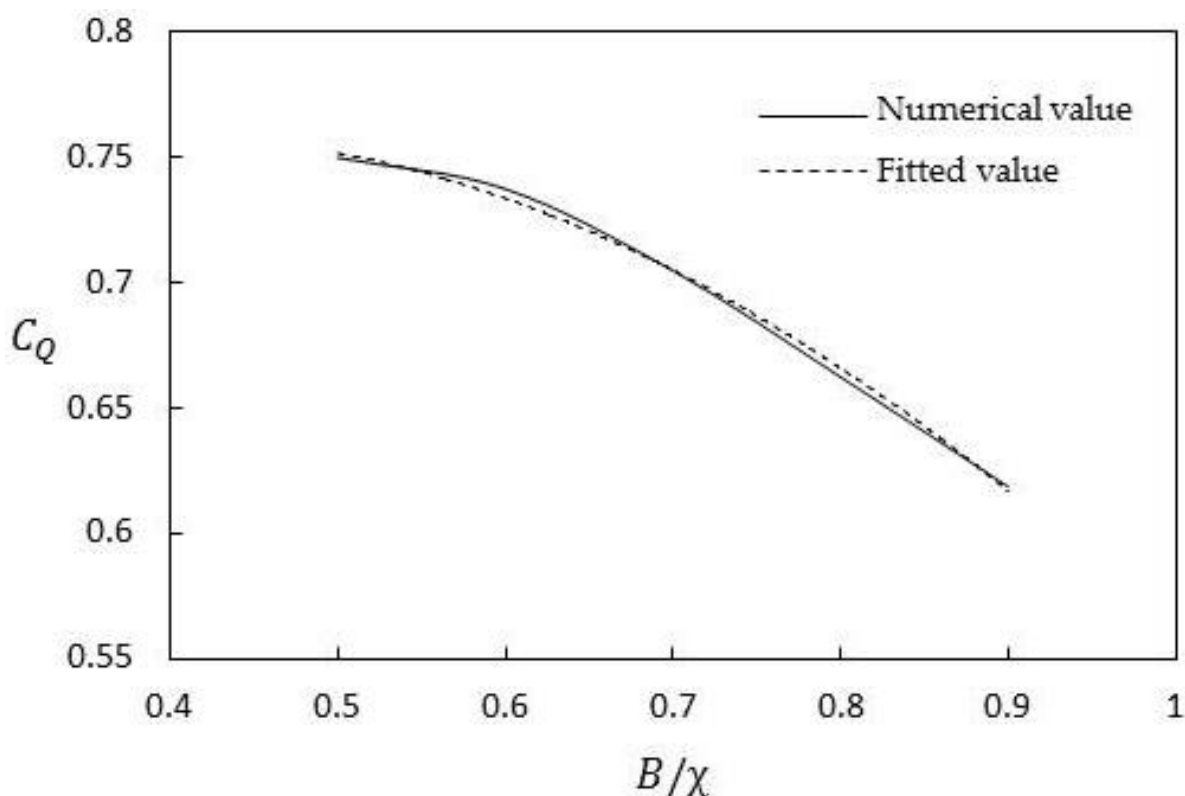


**Figure 8.**  $C_Q$  vs.  $B/\chi$  for laminar flow in rectangular open channels (data from numerical calculation).

#### 3.2. Experiments for Turbulence in an Open Channel

To study the discharge capacity parameter of turbulent flow in open channel with different cross-sectional shapes,  $B/\chi$  was chosen as another generalized parameter except hydraulic radius by referring to Equation (10). Based on the experimental data in this article and the experimental data from Tracy [19], Kirkgöz [20], and Tominaga [25], the discharge capacity parameter  $C_Q$ , defined in Equation (8), was calculated. Then, the  $C_Q \sim Re_R \sim B/\chi$  diagram was drawn, as shown in Figure 9. For rectangular open channels,  $C_Q$  decreased with the increase in Reynolds number  $Re_R$ . In addition, for turbulent flow at medium and low Reynolds numbers (Reynolds number  $< 10^5$ ) in different  $B/\chi$  conditions,  $C_Q$  were quite dispersed, showing that  $C_Q$  is clearly dependent on  $B/\chi$ , i.e., when  $B/\chi$  is different, the corresponding  $C_Q$  is also significantly different. However, after the Reynolds number reaches  $10^5$ , in different  $B/\chi$  conditions,  $C_Q$  is gradually concentrated into a line and the dependence of  $C_Q$  on  $B/\chi$  is weakened.  $C_Q$  values of different  $B/\chi$  values tended to overlap.  $C_Q$  showed a trend only related to the Reynolds number.

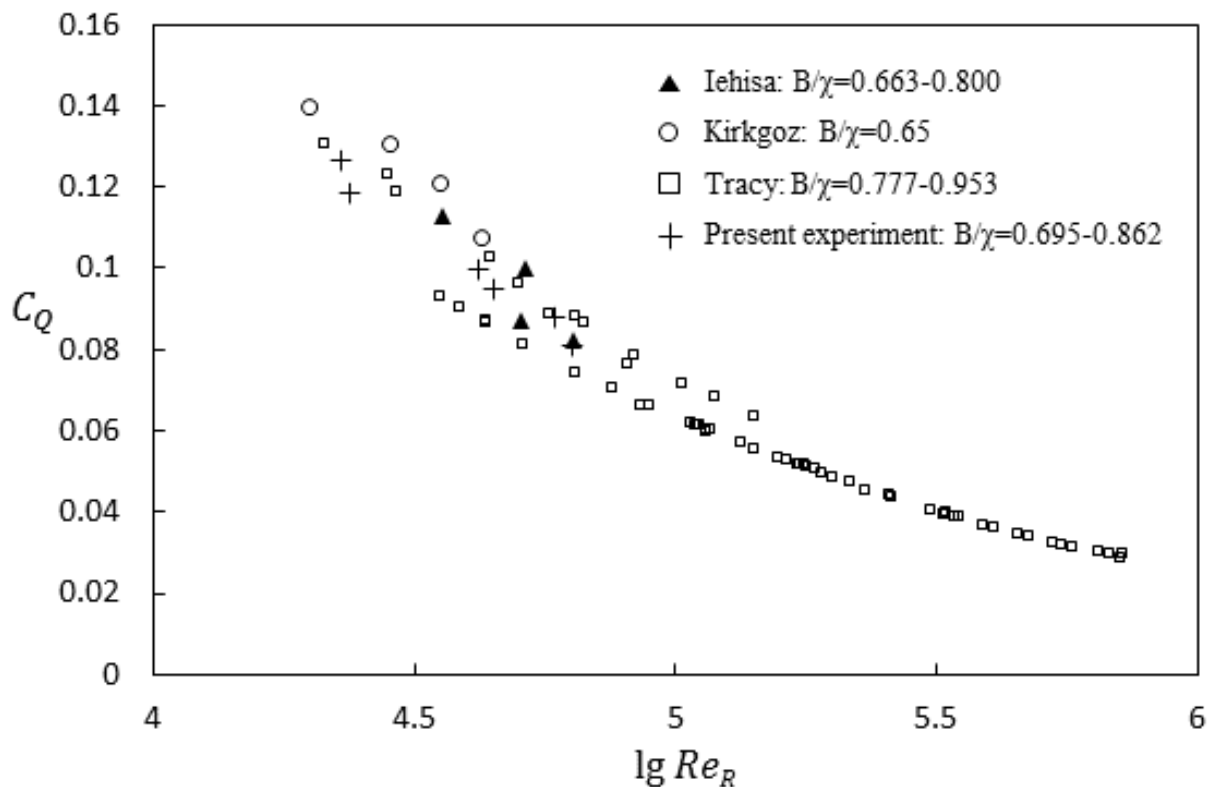


**Figure 9.**  $C_Q$  vs.  $Re_R$  for rectangular open channels with different  $B/\chi$  values (data from experiments).

### 3.3. Numerical Calculations

#### 3.3.1. Mathematical Model and Verification

The Reynolds time-mean equation is used to describe the flow movement of open channels. The governing equation includes a continuity equation and motion equation. The Reynolds stress transport model (RSM) is used to seal the above equations. In the numerical calculation, a hexahedral grid is used to divide the solution region. The finite volume method (FVM) is used to discretize the equations. In this process, the convection term adopts a first-order upwind scheme, and the diffusion term adopts a central difference scheme. Then, the discrete equation can be obtained. The SIMPLE algorithm based on a collocated grid is used to determine the coupling relationship between pressure and velocity. The Gauss–Seidel iterative method is used to solve algebraic equations. The convergence condition is set as the residual of inlet unit flow  $< 0.01\%$  and the residual of total flow  $< 0.5\%$ .

The experimental results in this paper were used to verify the calculations. The calculated time-mean velocity distribution agrees with the experimental results. Figure 10 only shows the comparison between the calculated results and experimental results in sections 2#, 3#, 4#, and 5# of experimental condition 3 in this paper due to space limitations. The resulting curves almost overlap. In each working condition, the experimental results are mostly in accordance with numerical results, which shows that the numerical results are accurate. Both sets of data presented a trend of logarithmic variation, i.e., the water depth decreased more slowly near the water surface and more rapidly near the bottom of the flume.

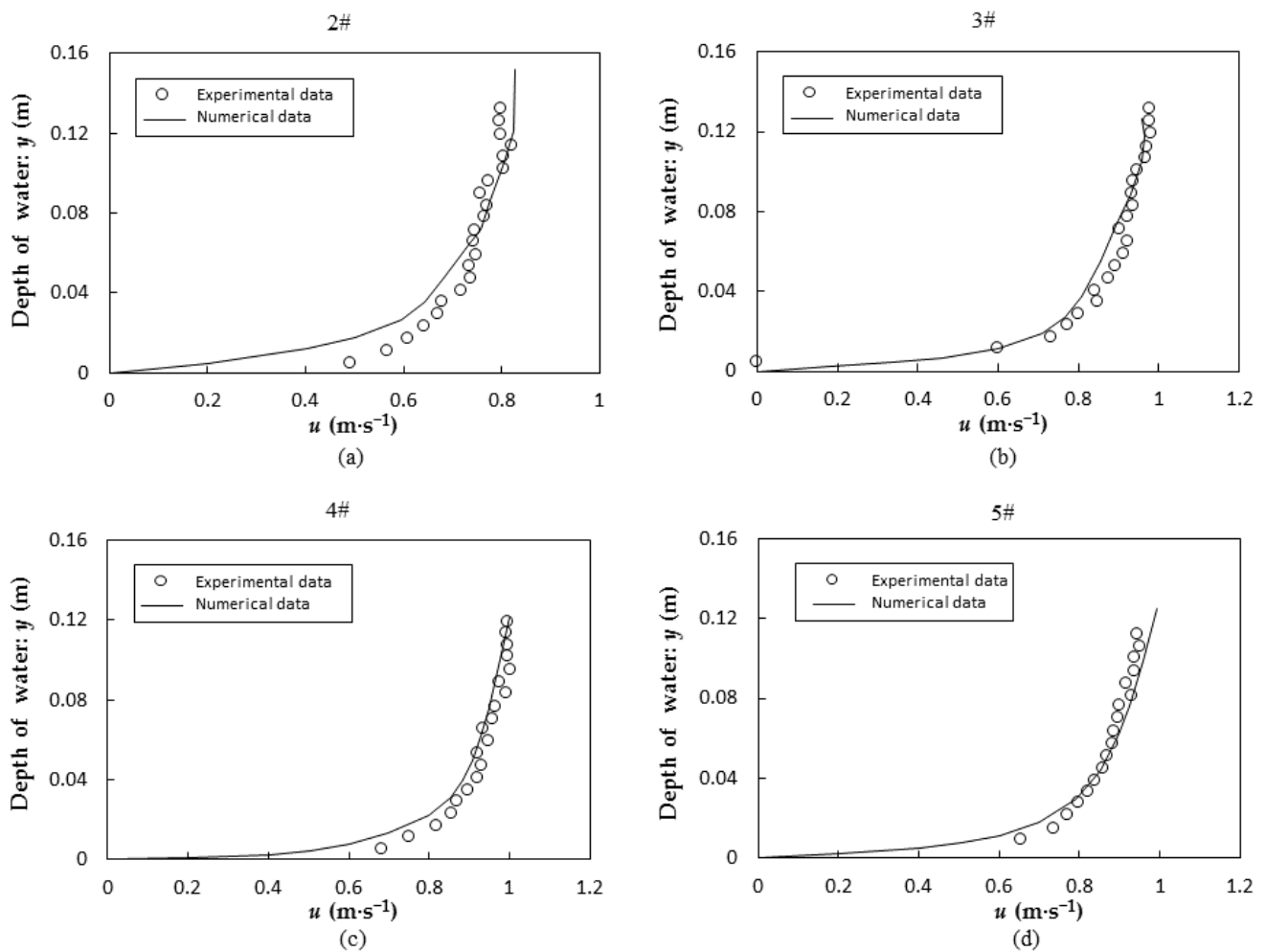


**Figure 10.** Velocity profiles of cross-sections in experimental condition 3 (data from experiment and numeric calculations): (a) 2# cross-section, (b) 3# cross-section, (c) 4# cross-section, and (d) 5# cross-section.

### 3.3.2. Rectangular Open Channel

Artificial water channels and natural river channels have various cross-sectional shapes. Artificial channels are mainly rectangular and trapezoidal, whereas natural channels are compound. Figure 11 shows the variation in discharge capacity parameters  $C_Q$  with Reynolds number and width-to-wetted perimeter ratio in a turbulent rectangular open channel. To facilitate comparison, the corresponding experimental results with high Reynolds number turbulent flow conditions are also shown. Figure 11 shows that, similar to the experimental results in Figure 9,  $C_Q$  decreased with increasing Reynolds number. In addition, for numerical values, when the Reynolds number is less than  $10^5$ ,  $C_Q$  is dispersed in different  $B/\chi$  conditions, indicating that  $C_Q$  still depends on  $B/\chi$ . If the Reynolds number is greater than  $10^5$ ,  $C_Q$  is concentrated and it is assumed that  $C_Q$  no longer depends on  $B/\chi$ . In a high Reynolds number region (Reynolds number greater than  $10^5$ ), the variation trend of experimental results and numerical results are consistent, which shows that  $C_Q$  can reflect the variation trend of the flow discharge capacity. However, the experimental values were slightly smaller than the numerical values. A possible reason for this is that the actual energy loss was not fully taken into account in the numerical calculation. Therefore, the numerical  $C_Q$  values were slightly higher.

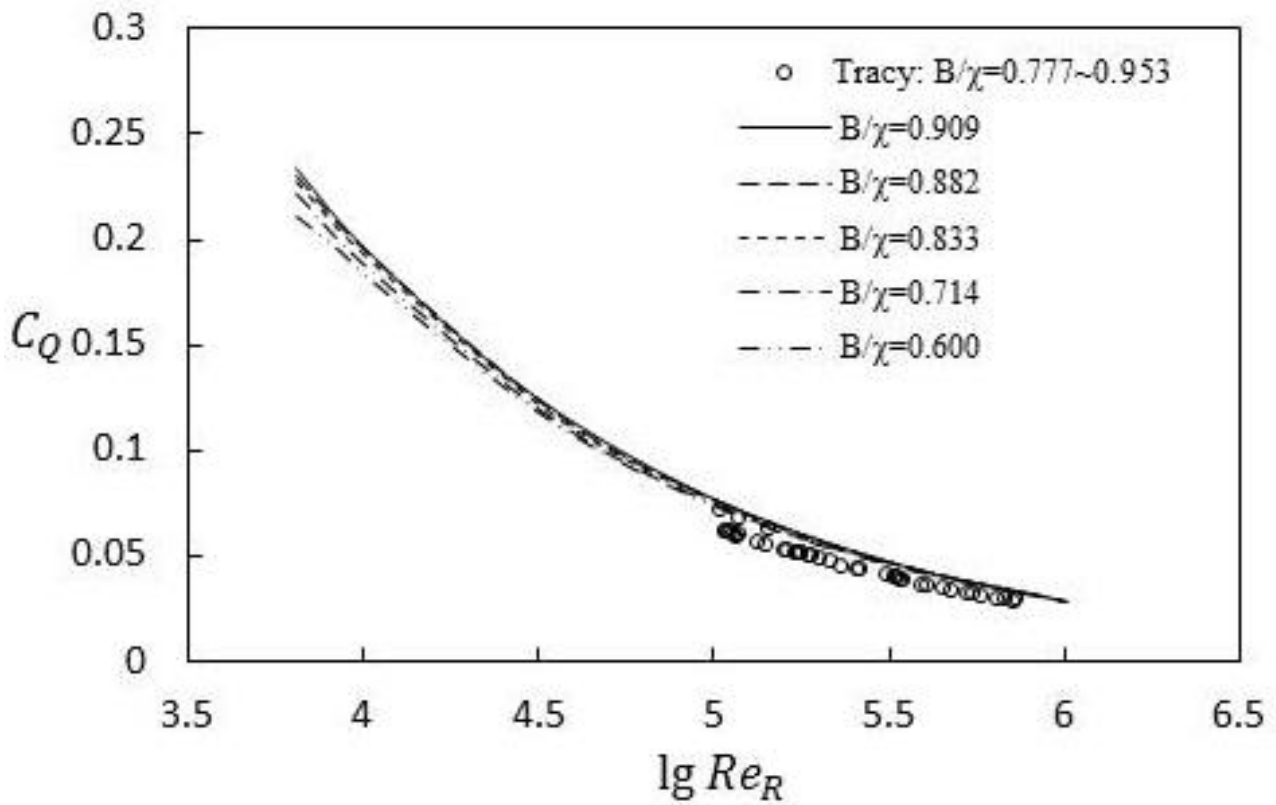


**Figure 11.**  $C_Q$  vs.  $Re_R$  for rectangular open channels with different  $B/\chi$  in turbulent flow (data from numerical calculation and Tracy et al. [19]).

### 3.3.3. Open Channels with Other Cross-sections

Figure 12 shows the generalization of cross-sections for trapezoidal open channels and compound open channels. Figures 13 and 14 show the variation in discharge capacity parameter with Reynolds number and width-to-wetted perimeter ratio. Regardless of the trapezoidal open channels or compound open channels,  $C_Q$  showed a similar trend to that of rectangular open channels: the  $C_Q$  value decreased with increasing Reynolds number and  $C_Q$  values were bounded by a Reynolds number of  $10^5$ , and  $C_Q$  showed strong dependence on  $B/\chi$  for turbulent flow at low and medium Reynolds numbers. However, in the case of high Reynolds number turbulent flow,  $C_Q$  was no longer dependent on  $B/\chi$ , but on the Reynolds number.

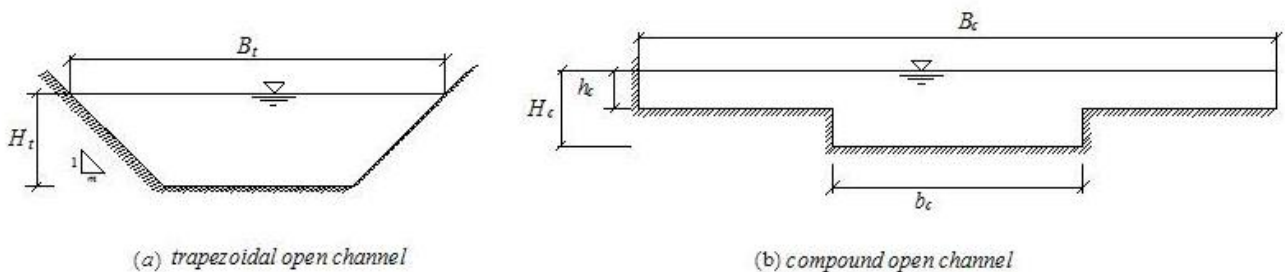


**Figure 12.** Sketch of open channels with different cross-sections: (a) trapezoidal open channel, (b) compound open channel.

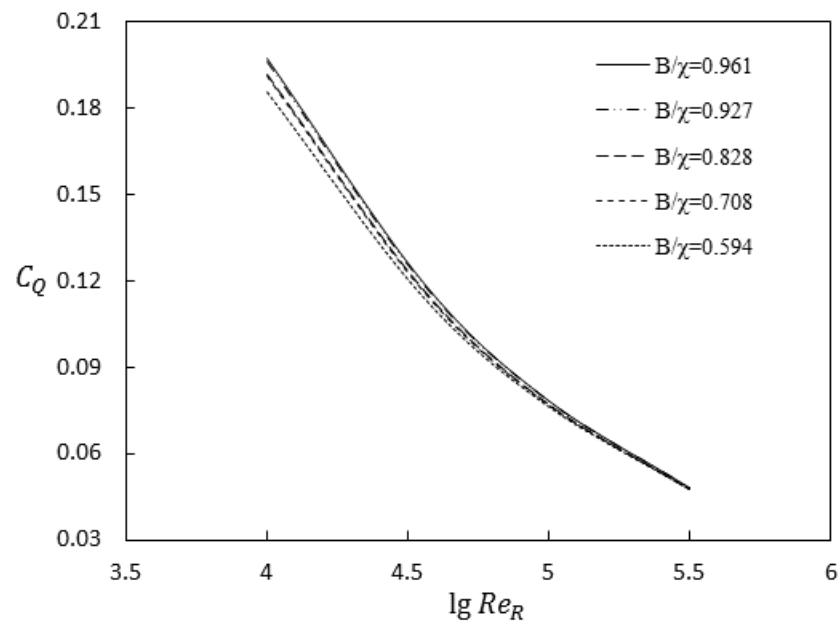


Figure 13.  $C_Q$  vs.  $Re_R$  for trapezoidal open channels with different  $B/\chi$  (data from numerical calculation).

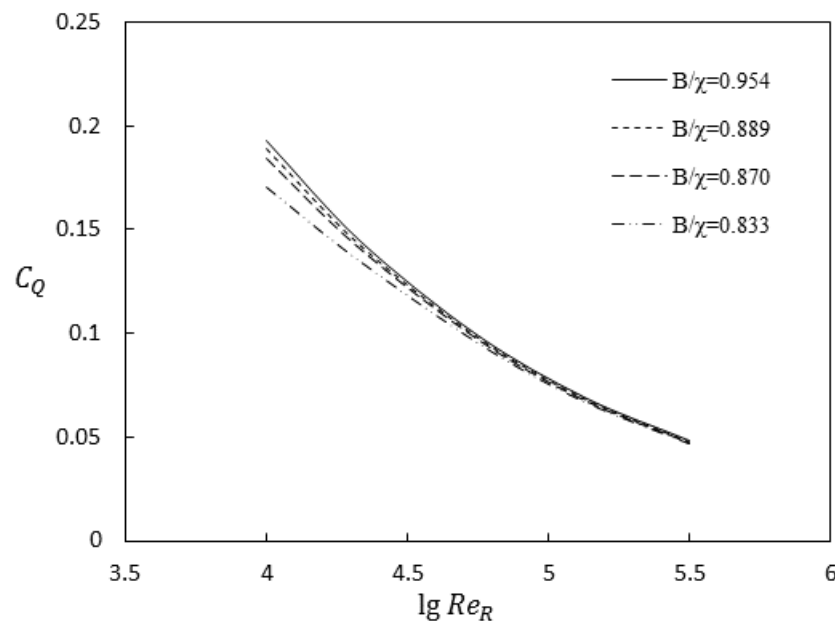


Figure 14.  $C_Q$  vs.  $Re_R$  for compound open channels with different  $B/\chi$  (data from numerical calculation).

#### 4. Discussion

To analyze the variation in the discharge capacity parameter  $C_Q$  in conditions with various cross-sectional shapes (rectangular, trapezoidal, and compound), the numerical results and experimental results for turbulent flow and theoretical solutions for laminar flow were combined into the same figure (all for open-channel flow). Figures 15 and 16 show the variation in  $C_Q$  with  $Re_R$  at a given width-to-wetted perimeter ratio ( $B/\chi$  is 0.7 and 0.9, respectively). Figures 15 and 16 show the following: (1) For medium and low Reynolds number turbulence with a Reynolds number less than  $10^5$  with the same  $B/\chi$  value, the  $C_Q$  of the three types of cross-sectional shapes (namely, rectangular, trapezoidal, and compound) were different from each other. The discharge capacity parameter  $C_Q$  varied with the shape of the cross-section, and the mechanism was extremely complex; further study is needed. (2) For turbulent flow with a high Reynolds number greater

than  $10^5$ , the numerical values of  $C_Q$  in the three cross-sectional conditions were almost the same as the experimental values, and  $C_Q$  was no longer dependent on the width-to-wetted perimeter ratio  $B/\chi$ . In high Reynolds number turbulent flow conditions, turbulence structures at different scales were fully developed, and the discharge capacity parameter,  $C_Q$ , was no longer dependent on the shape of the cross-section. The experimental and numerical results in Figures 15 and 16 are mostly consistent. However, the experimental values in Figure 16 were slightly lower than the numerical results. A possible reason for this is that the actual energy loss was not fully taken into account in the numerical calculations. Therefore, the numerical  $C_Q$  values were slightly higher.

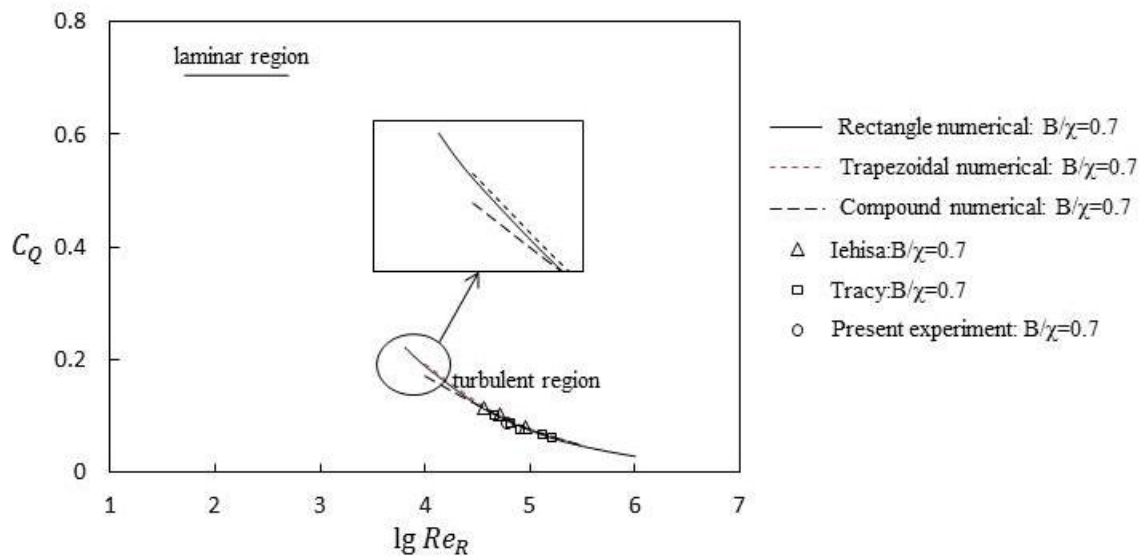


Figure 15.  $C_Q$  vs.  $Re_R$  for open channels with different cross-sections ( $B/\chi = 0.7$ ).

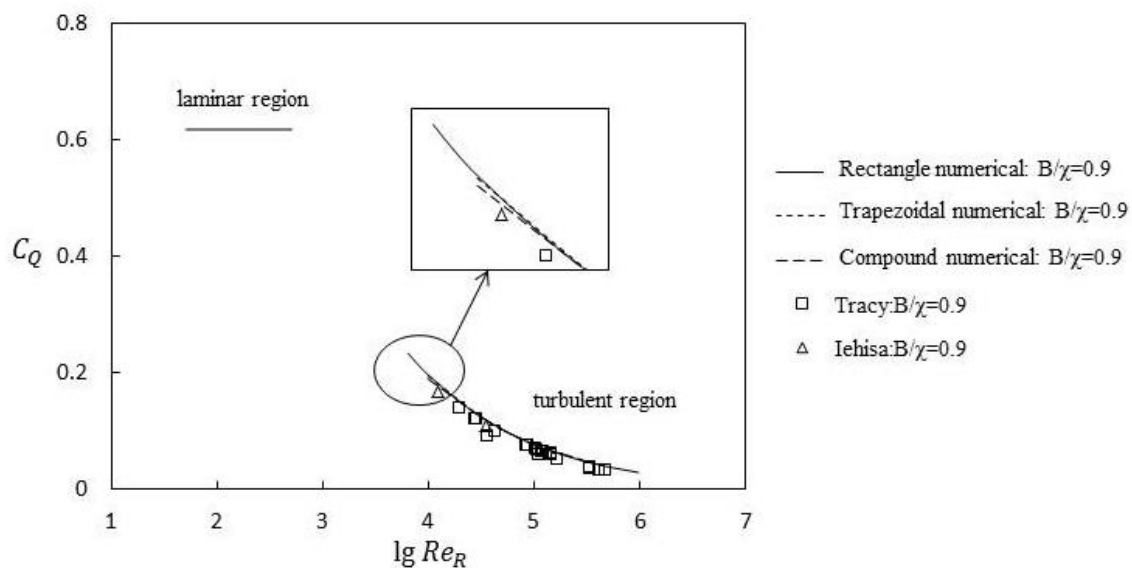


Figure 16.  $C_Q$  vs.  $Re_R$  for open channels with different cross-sections. ( $B/\chi = 0.9$ ).

The numerical results and experimental data were used to calculate  $\lambda$  values in laminar flow and turbulent flow with medium and high Reynolds numbers (Figures 17 and 18 for  $B/\chi = 0.7$  and  $B/\chi = 0.9$ , respectively). As can be seen in Figures 17 and 18,  $\lambda$  varied greatly in the laminar flow region. This indicates that  $\lambda$  was obviously affected by the Reynolds number in the laminar flow region. In turbulent regions with medium and high Reynolds numbers, in the experimental data and numerical data and regardless of the

shape of the cross-section (rectangle, trapezoidal, or compound shapes,  $B/\chi = 0.7$  or  $0.9$ ), the  $\lambda$  values basically coincided and did not change. The results show that  $\lambda$  did not depend on the Reynolds number in the middle and high Reynolds number turbulent region. The experimental and numerical results in Figures 17 and 18 are mostly consistent. However, the experimental values in Figure 18 were slightly higher than the numerical results. A possible reason for this is that the actual energy loss was not fully taken into account in the numerical calculations. Therefore, the energy loss values from the numerical calculations were lower.

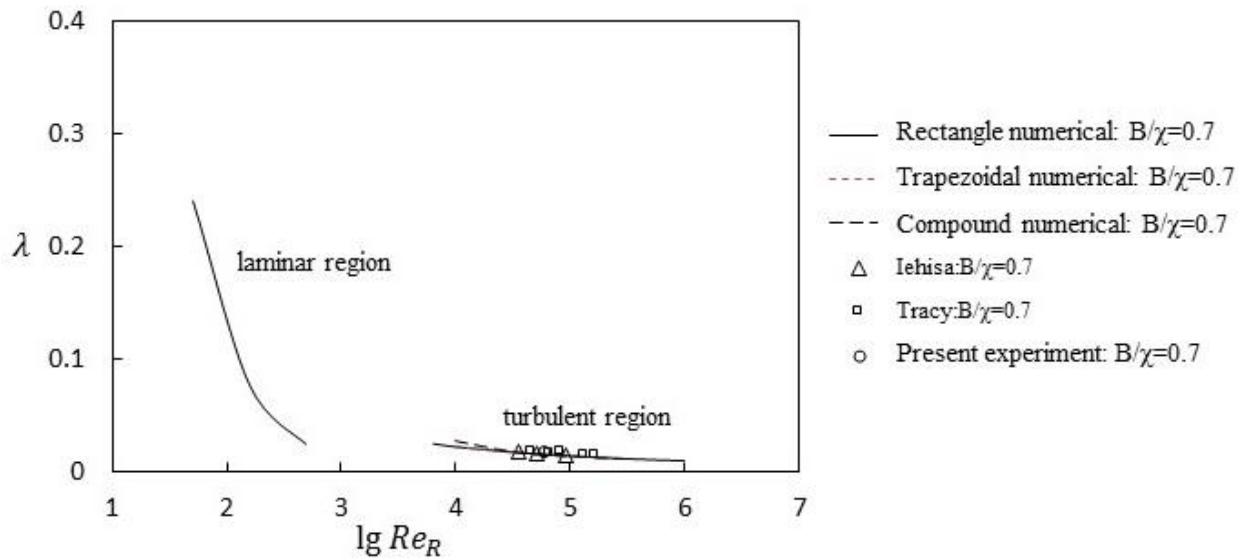


Figure 17.  $\lambda$  vs.  $Re_R$  for open channels with different cross-sections ( $B/\chi = 0.7$ ).

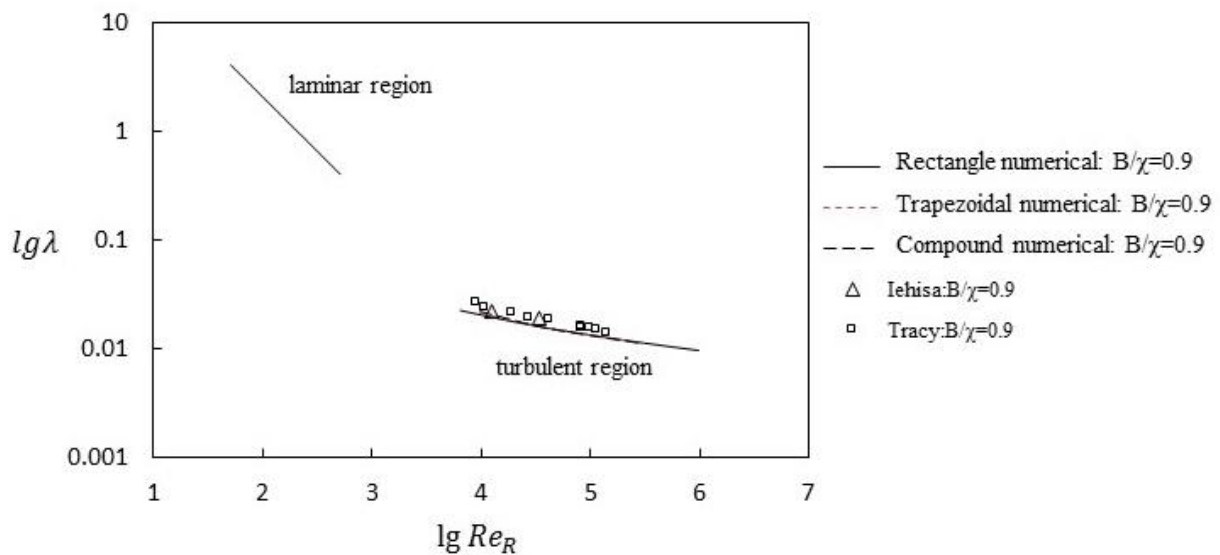


Figure 18.  $\lambda$  vs.  $Re_R$  for open channels with different cross-sections ( $B/\chi = 0.9$ ).

### 5. Conclusions

Through theoretical analysis, experimental research, and numerical calculations, the influence of cross-sectional shape on the discharge capacity of an open channel was studied. The conclusions are as follows:

- (1) The expression of the discharge capacity of an open channel was proposed under the framework of the viscous liquid motion theory. A parameter  $C_Q$  affecting the discharge capacity of laminar flow and turbulent flow in open channels with different types of cross-sections was obtained.

(2) Width-to-wetted perimeter ratio can be used to generalize the cross-section of open channels. The dependence of the discharge capacity on the shape of the cross-section was shown as follows: in laminar flow, the parameter  $C_Q$  was only related to the width-to-wetted perimeter ratio. For medium and low Reynolds number turbulence, parameter  $C_Q$  varied with the Reynolds number and width-to-wetted perimeter ratio. However, for high Reynolds number turbulent flow, the discharge capacity parameter  $C_Q$  did not vary with width-to-wetted perimeter ratio.

**Author Contributions:** Conceptualization, C.Q., S.L., W.P. and R.X.; methodology, C.Q., S.L., W.P. and R.X.; formal analysis, C.Q., S.L., W.P. and R.X.; investigation, C.Q., W.P. and R.X.; resources, C.Q., W.P. and R.X.; data curation, C.Q., W.P. and R.X.; writing—original draft preparation, C.Q., W.P. and R.X.; writing—review and editing, C.Q., S.L., W.P. and R.X.; visualization, C.Q., W.P. and R.X.; supervision, S.L. and J.H.; project administration, S.L.; funding acquisition, S.L. All authors have read and agreed to the published version of the manuscript.

**Funding:** This research was funded by the National Key R&D Program of China, Ministry of Science and Technology of the People’s Republic of China, grant number 2018YFC0407600.

**Data Availability Statement:** The data presented in this study are available on request from authors.

**Acknowledgments:** The authors would like to express their gratitude to Changjiang River Scientific Research Institute.

**Conflicts of Interest:** The authors declare no conflict of interest.

## References

- Graf, W.H.; Altinakar, M.S.; Zhao, W.Q.; Wan, Z.H. *Hydraulique Fluviale*; University of Electronic Technology of China Press: Chengdu, China, 1997. (In Chinese)
- Carter, R.W.; Einstein, H.A.; Hinds, J.; Powell, R.W.; Silberman, E. Friction Factors in Open Channels: Progress Report of the Task Force on Friction Factors in Open Channels of the Committee on Hydromechanics of the Hydraulics Division. *J. Hydraul. Div.* **1963**, *89*, 97–143.
- Cantero, F.; Castro-Orgaz, O.; Garcia-Marín, A.; Ayuso, J.L.; Dey, S. Free surface profiles in river flows: Can standard energy-based gradually-varied flow computations be pursued? *J. Hydrol.* **2015**, *529*, 1644–1656. [[CrossRef](#)]
- Chow, V.T. *Open Channel Hydraulics*; McGraw-Hill: New York, NY, USA, 1959.
- Prinos, P.; Townsend, R.D. Comparison of methods for predicting discharge in compound open channels. *Adv. Water Resour.* **1984**, *7*, 180–187. [[CrossRef](#)]
- Dracos, T.; Hardegger, P. Steady uniform flow in prismatic channels with flood plains. *J. Hydraul. Res.* **1987**, *25*, 169–185. [[CrossRef](#)]
- French, R.H. *Open Channel Hydraulics*; McGraw-Hill: New York, NY, USA, 1987.
- Wormleaton, P.R.; Allen, J.; Hadjipanous, P. Discharge assessment in compound channel flow. *J. Hydraul. Div.* **1982**, *108*, 975–994. [[CrossRef](#)]
- Khatua, K.K.; Patra, K.C.; Mohanty, P.K. Stage-Discharge prediction for straight and smooth compound channels with wide floodplains. *J. Hydraul. Eng.* **2011**, *138*, 93–99. [[CrossRef](#)]
- Blalock, M.E.; Sturm, T.W. Minimum specific energy in compound open channel. *J. Hydraul. Div.* **1981**, *107*, 699–717. [[CrossRef](#)]
- Field, W.G.; Lambert, M.F.; Williams, B.J. Energy and momentum in one dimensional open channel flow. *J. Hydraul. Res.* **1998**, *36*, 29–42. [[CrossRef](#)]
- Chaudhry, M.; Bhallamudi, S. Computation of critical depth in symmetrical compound channels. *J. Hydraul. Res.* **1988**, *26*, 377–396. [[CrossRef](#)]
- Blalock, M.E.; Sturm, T.W. Closure to minimum specific energy in compound open channel. *J. Hydraul. Eng.* **1983**, *109*, 483–487. [[CrossRef](#)]
- Costabile, P.; Macchione, F. Analysis of one-dimensional modeling for flood routing in compound channels. *Water Resour. Manag.* **2012**, *26*, 1065–1087. [[CrossRef](#)]
- Johnson, E.D.; Cowen, E.A. Remote monitoring of volumetric discharge employing bathymetry determined from surface turbulence metrics. *Water Resour. Res.* **2016**, *52*, 2178–2193. [[CrossRef](#)]
- Harpold, A.A.; Mostaghimi, S.; Vlachos, P.P.; Brannan, K.; Dillaha, T. Stream discharge measurement using a large-scale particle image velocimetry (LSPIV) prototype. *Trans. ASABE* **2006**, *49*, 1791–1805. [[CrossRef](#)]
- Chen, C.I. Unified theory on power laws for flow resistance. *J. Hydraul. Eng. ASCE* **1991**, *117*, 371–389. [[CrossRef](#)]
- Schlichting, H.; Gersten, K.; Krause, E.; Oertel, H. *Boundary-Layer Theory*; McGraw-Hill: New York, NY, USA, 1960; Volume 7.
- Tracy, H.J.; Lester, C.M. *Resistance Coefficients and Velocity Distribution Smooth Rectangular Channel*; US Government Printing Office: Washington, DC, USA, 1961.

20. Kirkgöz, M.S. Turbulent velocity profiles for smooth and rough open channel flow. *J. Hydraul. Eng.* **1989**, *115*, 1543–1561. [[CrossRef](#)]
21. Liu, S.H.; Xue, J.; Fan, M. The calculation of mechanical energy loss for incompressible steady pipe flow of homogeneous fluid. *J. Hydrodyn.* **2013**, *25*, 1912–1918. [[CrossRef](#)]
22. Liu, S.H.; Fan, M.; Xue, J. The mechanical energy equation for total flow in open channels. *J. Hydrodyn.* **2014**, *26*, 416–423. [[CrossRef](#)]
23. Liu, S.H.; Xue, J. Theoretical analysis and numerical simulation of mechanical energy loss and wall resistance of steady open channel flow. *J. Hydrodyn.* **2016**, *28*, 416–423. [[CrossRef](#)]
24. Zhao, Q.Y.; Liu, S.H.; Liao, W.J. Study of total flow control equations and energy loss characteristics of steady turbulent flow in open channel. *Adv. Water Sci.* **2020**, *31*, 270–277.
25. Tominaga, A.; Nezu, I.; Ezaki, K.; Nakagawa, H. Three-dimensional turbulent structure in straight open channel flows. *J. Hydraul. Res.* **1989**, *27*, 149–173. [[CrossRef](#)]

**Disclaimer/Publisher’s Note:** The statements, opinions and data contained in all publications are solely those of the individual author(s) and contributor(s) and not of MDPI and/or the editor(s). MDPI and/or the editor(s) disclaim responsibility for any injury to people or property resulting from any ideas, methods, instructions or products referred to in the content.